Chapter

# Full-Color Micro-LED Devices Based on Quantum Dots

*Tingzhu Wu, Tingwei Lu, Yen-Wei Yeh, Zhong Chen and Hao-Chung Kuo*

## Abstract

Quantum dots (QDs) show remarkable optical and electrical characteristics. They offer the advantage of combining micro-LEDs (μLEDs) for full-color display devices due to their exceptional features. In addition, μLED used in conjunction with QDs as color-conversion layers also provide efficient white LEDs for high-speed visible light communication (VLC). In this article, we comprehensively review recent progress in QD-based μLED devices. It includes the research status of various QDs and white LEDs based on QDs' color conversion layers. The fabrication of QD-based high-resolution full-color μLEDs is also discussed. Including charge-assisted layer-by-layer (LbL), aerosol jet printing, and super inkjet printing methods to fabricate QD-based μLEDs. The use of quantum dot photoresist in combination with semipolar μLEDs is also described. Finally, we discuss the research of QD-based μLEDs for visible light communication.

**Keywords:** quantum dots, micro-LEDs, full-color displays, visible light communication

## 1. Introduction

Light-emitting diodes (LED) have been widely used in daily life due to their advantages of high efficiency, energy saving, and long working life, such as lighting sources, full-color displays, and backlight sources of liquid crystal displays [1]. Recently, mobile device displays, such as smart furniture, augmented reality (AR), virtual reality (VR), and wearable devices have piqued extensive attention from the semiconductor industries and research on micro-LEDs (μLEDs), which are referred to as chips with sizes less than $50 \times 50\ \mu m^2$ [2]. Due to their excellent properties in terms of brightness, lifetime, resolution, and efficiency, μLEDs have been considered the most promising next-generation display technologies [3]. The potential of μLEDs to replace conventional display technologies is owing to the combination of their self-emissive mechanism and inorganic material characteristics. Over the past decade, the number of commercially available μLED displays has grown significantly, as manufacturers seek to capitalize on the success of this technology. Sony introduced its first 55-inch full high-definition (HD) μLED TV panel with 1920 × 1080 resolution in 2012, which consists of over 6 million individual μLEDs. Samsung unveiled the world's first consumer modular μLED 146-inch TV in 2018, which is named "The

Wall." In 2022, Samsung will launch a new μLED TV with 25 million pixels, providing vivid colors,high definition, and contrast, and also supports 20-bit grayscale depth, more than 1 million levels of brightness and color. In the academic field, μLEDs have been studied for more than 10 years.

In addition to displays, μLEDs have recently been adopted as transmitters in visible light communication (VLC) systems, based on their quick response times [4]. Currently, radio frequency (RF) communication faces some challenges, such as interference, bandwidth limitations, security issues, transmission power limitations, and power inefficiency [5]. VLC is an emerging technology that addresses the crowded radio spectrum, using visible light to communicate to enable high-speed internet connections. As a light source that is harmless to human body, LED can have both lighting and communication functions when used in VLC, which can save extra power [6].

The modulation bandwidth of an LED is constrained by the carrier lifetime and the time constant consisting of capacitance of a depletion layer and junction differential resistance. Due to their small size, μLEDs can withstand higher injection current densities, thereby enabling smaller carrier lifetimes and higher modulation bandwidths. In addition, a smaller active area will reduce the geometric capacitance of the device, thereby reducing the RC time constant. In addition, μLEDs also have better current uniformity, which will also increase the modulation bandwidth featuring exclusive properties making μLEDs widely applicable for high-speed VLC system.

## 2. Full-color μLED display based on quantum dots

### 2.1 Background of full-color μLED display

The commonly used full-color strategy is employing the combination of red–green–blue (RGB) μLED devices in a display. However, this approach has a number of drawbacks. First, the so-called "green gap" created by green μLEDs results in low efficiency [7]. For green LEDs, a high proportion of indium is required in the active region, which requires relatively low growth temperatures, resulting in poor crystal quality of the LED epitaxial layers. In addition, high proportions of indium produce strong polarization fields in InGaN/GaN multiple quantum wells (MQWs) and lead to strong quantum-confined Stark effects, reducing recombination efficiency [7]. Also, red μLEDs are problematic. The active region of the red LED consists of AlGaInP material, which has a high surface recombination velocity (~$10^6$ cm/s) [8], coupled with a long carrier diffusion length of about a few microns, making non-radiative surface recombination much more efficient [9]. Therefore, as the device size shrinks to a few microns, the EQE degradation of red μLEDs is more severe than that of blue and green μLEDs. Another problem in the RGB μLED strategy is the mismatch of drive voltages between RGB pixels. The threshold voltage of the blue LED is about 3.3 V, while the threshold voltages of the red and green LEDs are 1.7 and 2.2 V, which complicates the driver circuit design.

To address these issues, blue μLEDs can be integrated with color converters, such as yellow-emitting phosphors or red and green-emitting nanocrystals (NCs), for higher-quality full-color displays [10]. To date, extensive research and development have been carried out on phosphor materials for PC-LEDs. Lin. Wait. Successfully fabricated high luminance efficiency and wide color gamut for NC-based solid-state and hybrid WLED devices, which exhibited higher efficiency (51 lm $W^{-1}$), wide color gamut (122% of NTSC and 91% of Rec. 2020), and the efficiency decays by about 12% during the 200-h reliability test [11]. However, organic or inorganic phosphors are generally not suitable for μLED displays due to their spectral width and asymmetry, inherent instability, low red phosphor efficiency, down conversion energy loss, and low absorption cross-section in the blue/UV wavelength region [12]. In addition, the particle size of conventional phosphors may be comparable to or larger than that of μLED chips, which will affect device performance.

### 2.2 QD-based color conversion for μLEDs

Quantum dots (QDs) are nanoscale semiconductor crystals, and whose electrical and optical properties can be tuned by changing their sizes [13, 14]. Compared with traditional fluorophores, several QD photophysical properties are distinct and unmatched. The first is the ability to tune photoluminescence emission according to the core size and quantum confinement effects of semiconductor binary combinations. This unique advantage allows one to control the emission properties of QDs by controlling the core size [1]. In addition, QDs have broad absorption spectra, starting with blue emission and then steadily increasing towards UV. As combined with the aforementioned properties, quantum dots have emerged as omnidirectional attractive fluorophores for full-color displays.

Core-type QDs, such as CdSe, CdS, or CdTe, are the most studied and commercialized QDs due to their excellent optical and electrical properties [15, 16]. Using these precursors, high fluorescence quantum yields of up to 80% have been reported [17, 18]. However, many heavy metal elements are contained in such quantum dots, and Core-type QDs will pollute the environment, which limits their wide application. To prevent the use of toxic metal elements for the persistent development of QD-based products, the fabrication of Cd/Pb-free QDs has become a subject of intense interest in recent years. In 2020, Soheyli et al. reported a novel aqueous-phase approach for the preparation of multicomponent In-based QDs. Absorption and photoluminescence emission spectra of the as-prepared QDs were tuned by alteration of QDs' composition as Zn-Ag-In -S/ZnS, Ag-In-S/ZnS, and Cu-Ag-In-S/ZnS core/shell QDs [19]. However, such materials have extremely small color gamut and color purity and are not suitable for display applications [20].

As an environmentally benign material belonging to the III–V group semiconductor, InP is deemed as another promising candidate to replace Cd/Pb-based QDs [21]. InP QDs are typical III–V group semiconductor nanocrystals that feature large excitonic Bohr radius and high carrier mobility [22]. Owing to the merits of low toxicity, high QYs, and broad color tunability, InP QDs are particularly suitable to construct LEDs for indoor/outdoor illumination, traffic signaling, and liquid-crystal display backlighting [23]. In general, InP QDs can be applied in μLEDs either as a photoluminescent layer or an electroluminescent layer. In 2015, Zhang et al. demonstrated a single "cadmium-free" component system consisting of Cu-doped InP core/ZnS barrier/InP quantum well/ZnS shell QDs [24]. These QDs exhibit two emission peaks by controlling the barrier thickness under single-excitation wavelength, one of which is attributed to Cu-doped InP, and the other resulting from InP quantum well. Using optimal structures as color converters, the WLED was obtained with a color rending index (CRI) up to 91 and CIE color coordinates of (0.338, 0.330) by combination with blue LED chip.

The metal halide perovskites QDs (PQDs) are considered the next generation thin-film LED light emitters because of their outstanding characteristics compared to colloidal QDs, which are derived from their narrower FWHM (below 30 nm) [25]. Tunable narrow and symmetrical PL peaks in the visible spectral range can be achieved by tuning the halide composition in perovskite materials. This property yields greater color purity, higher photoluminescence quantum yield (approaching 100%), more convenient synthesis, and lower manufacturing costs than conventional QDs [26]. In addition, PQDs have short carrier recombination lifetimes, which also lays the foundation for their application in the development of white-light VLC systems with high modulation bandwidth [27]. The ability to easily handle colloidal PQDs in solution enables the production of cost-effective large-area light-emitting layers [28]. Therefore, PQDs have been extensively studied in electronic and optoelectronic applications, such as photodetection, photovoltaics, and photoemission; especially as active materials or color converters in LEDs. To date, various PQD-based white LEDs have been reported using diverse structural designs that feature different advantages and disadvantages. However, due to poor thermal resistance and instability under high energy radiation, most PQD-based white light-emitting diodes (WLEDs) show only modest luminous efficiency of approximately 50 lm/W and a short lifetime of <100 h.

In 2019, Kang et al. demonstrated a new type of PQD film called PQD paper by using cellulose nanocrystals (CNCs) [29]. **Figure 1(a)** schematically shows the fabrication process of the PQD paper. The CNC suspension and $CH_3NH_3PbBr_3$ are combined in dimethylformamide, upon which the mixture is dried on the membrane to produce the PQDs paper. As shown in **Figure 1(b)**, the entangled CNC structure was clearly demonstrated by SEM. With the help of the CNC structure, the PQD paper performs the flexibility and unique mechanical strength. The size of the PQDs was $\approx 3^{-8}$ nm, which can enhance the light emission of perovskite by the provided strong quantum confinement, as shown in **Figure 1(c)**. **Figure 1(d)** illustrates the flux and current-dependent luminous efficiency of the PQD paper-based LED, the inset shows the emission of white LED. It can be clearly observed that the PQD paper-based LED has an ultrahigh luminous efficiency of 124 lm $W^{-1}$ and still exhibits a luminous efficiency of over 100 lm $W^{-1}$ even when the drive current increases to 50 mA. Moreover, after continuously working for 240 h, the PQD paper-based LED can maintain 87.6% luminous flux. Compared to the normal flat design, by using curved PQD paper, the viewing angle of LED was increased from 120° to 143° benefiting from the flexible nature of paper. This work also shows the fabricated white LEDs have a wide color gamut of 123% of NTSC standard and 92% of Rec. 2020, as shown in **Figure 1(e)**.

### 2.3 Fabrication of QD-based μLEDs for high-resolution displays

QD-based display technology has proven to be ideal for next-generation displays. In order to meet the needs of achieving high-resolution display, RGB QDs with sufficiently high pixel density need to be deposited on top of the substrate surface of μLED array. The μLED device realized in this way can replace the traditional OLED or LCD display to realize an ultra-high-definition display, for example, to meet the needs of AR/VR or ultra-high-definition TV. QD deposition and patterning techniques on a selected area of a substrate remain the major bottlenecks in realizing such devices. Therefore, in recent years, researchers have been exploring facile and efficient QDs patterning techniques, such as spray coating, aerosol jet printing, super-inkjet printing, etc.

To accurately locate QDs on the μLED array, the inkjet printing (IJP) has become a key technology for realizing QD-LED display. In 2015, Han et al. combined ultraviolet (UV) μLED and colloidal QDs to achieve a full-color display. RGB QDs were deposited on an array of GaN-based UV μLEDs with the help of an aerosol inkjet

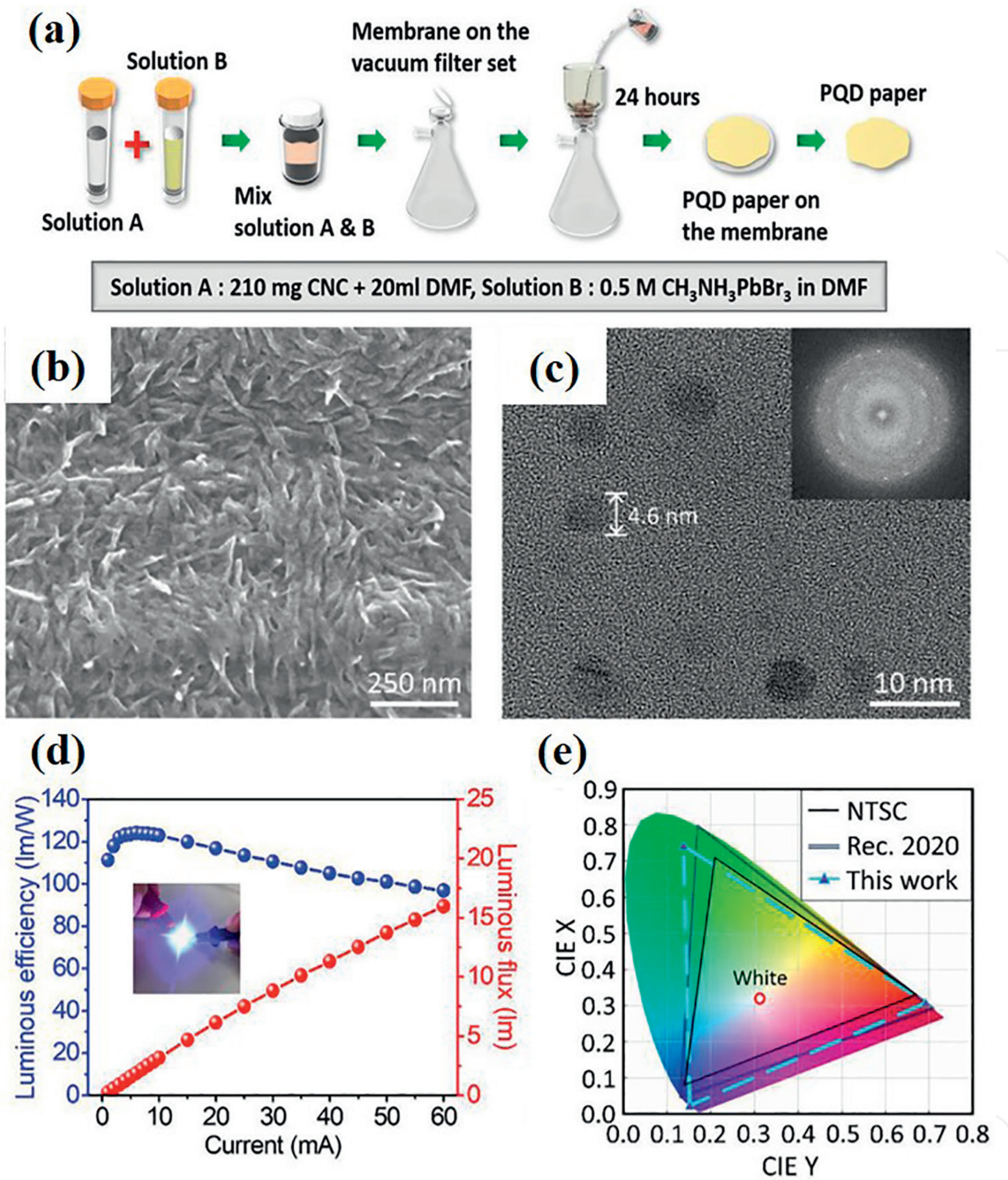


**Figure 1.**
*(a) Schematic of the fabrication process of the PQD paper. (b) SEM image of the PQD paper surface. (c) TEM image of the $CH_3NH_3PbBr_3$ PQDs obtained from the paper. The electron diffraction pattern in the inset reveals the high crystallinity of the PQDs. (d) Current-dependent luminous efficiency and luminous flux of the PQD paper-based LED. The inset shows the emission of white LED. (e) CIE diagram illustrating the color gamut of the NTSC standard, the Rec. 2020 standard, and the PQD paper-based LED [29]. Figure reproduced with permission from John Wiley and Sons.*

printer to ensure fine printing that is highly precise and mask-less and to enable noncontact deposition of liquids containing functional materials [30]. MQWs μLED arrays are grown on sapphire substrates. The UV micro-LED array is fabricated on a UV epitaxial wafer with a peak wavelength of 395 nm. Since pixels in the same column share an electrode of n-type GaN, the GaN is dry-etched into the sapphire substrate to create isolation trenches to isolate all micro-LED arrays. When the array is complete, the RGB QDs are sequentially sprayed onto the microLED array using

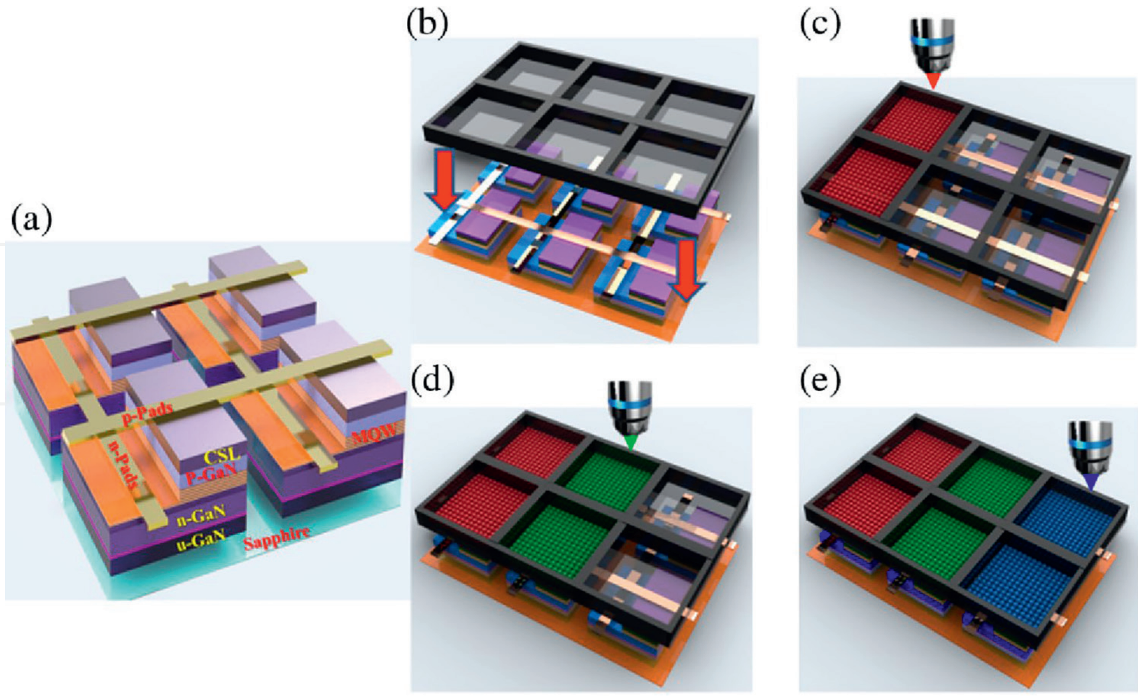


**Figure 2.**
*Process flow of the full-color microdisplay. (a) The structure of the micro-LED arrays. (b) Aligning the mold to the UV micro-LED array. (c)–(e) Consequently jetting the RGB QDs inside the molded window to form the full-color pixels [31]. Figures reproduced with permission from Optica Publishing Group.*

aerosol jet printing. The concentration of RGB QDs is about 5 mg/ml. Among the process parameters of aerosol jet printing, the working distance, table speed, carrier gas flow, sheath gas flow, and atomization frequency need to be adjusted to obtain a spraying line width of 35 μm. The working distance and table speed between the nozzle and the substrate were 1 mm and 10 mm/s, respectively. However, the cross-talk effect still occurred during the QD deposition due to the overflow of QDs during the solvent evaporation. To address the problem of cross-talk during QD deposition, the position of the QD must be restricted. In 2017, Lin et al. demonstrated a significant reduction in the cross-talk effect during the AJ printing process by using a photoresist (PR)-defined mold with a blocking wall to confine QDs [31]. **Figure 2** shows the fabrication process of the monolithic device. First, UV micro-LED arrays were fabricated on UV wafers with a peak wavelength of 395 nm and a pitch size of 40 μm. Isolation trenches are formed by etching GaN on a sapphire substrate. Through the dry etching process, $SiO_2$ is used as a hard mask. Finally, p-electrode stripes are defined on top of the chip, n-electrode stripes are defined on the n-GaN layer, and all pixels in the same row are connected. By aligning the window of the mold with the micro-LED mesa, as shown in **Figure 2(b)–(e)**, AJ RGB QDs can be efficiently deposited on the micro-LED mesa area without overlapping the trench area. The printing parameters of different quantum dots need to be optimized. For blue QDs, the working distance is 1 mm, the carrier gas flow rate is 66 sccm, the sheath gas flow rate is 11 sccm, and the stage speed is 10 mm/s. For green QDs, the working distance is 1 mm, the carrier gas flow rate is 72 sccm, the sheath gas flow rate is 15 sccm, and the stage speed is 10 mm/s. For red QDs, the working distance is 1 mm, the carrier gas flow rate is 83 sccm, the sheath gas flow rate is 17 sccm, and the stage speed is 10 mm/s.

Pixels of an RGB display are demonstrated after depositing QDs on micro-LEDs using AJ on a die that has been window-confined. **Figure 3(a)** shows the microscope

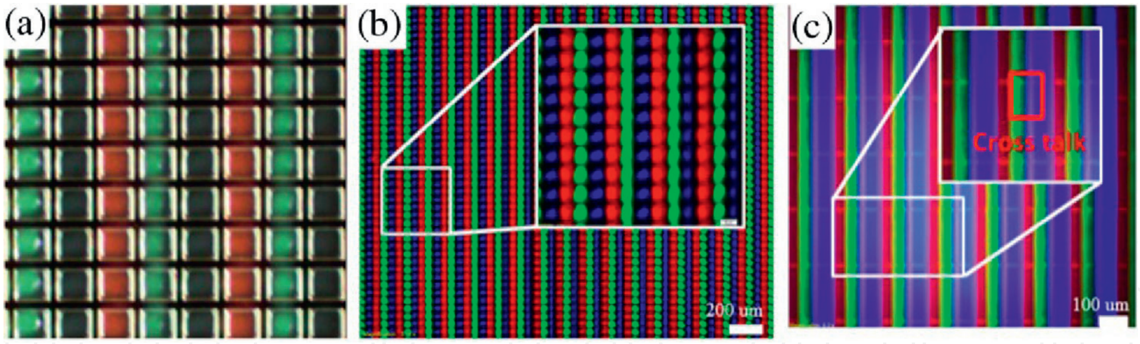


**Figure 3.**
*(a) Microscope image of the full-color micro-LED after jetted QDs in the PR mold. (b) The RGB pixel array observed by fluorescence microscopy. (c) The fluorescence microscopy image of the jetted QD pixels without the PR mold [31]. Figures reproduced with permission from Optica Publishing Group.*

image of the full-color micro-LED after jetted QDs in the PR mold. **Figure 3(b)** shows the RGB pixel array observed by fluorescence microscopy, indicating that the luminescent regions of quantum dots have clear boundaries. Compared with the result of printing without PR window restriction as shown in **Figure 3(c)**, the fluorescence image shows no obvious separation between the printed QDs. Clearly, crosstalk is observed in the blue QD lines.

In 2019, Chen et al. proposed hybrid QD nanoring μLEDs (QD-NR-μLEDs) fabricated by QD printing and electron beam (E-beam) lithography [32]. There are three parts to this device, namely, a normal green LED, a blue NR-μLED, and a red QD-NR-μLED, and each region can be regarded as a subpixel, as shown in the SEM images of **Figure 4(a)**. Besides, the nonradiative resonant energy transfer (NRET) mechanism was allowed for adjacent coupling between the exposed InGaN/GaN MQW sidewalls and QDs. During the manufacturing process, an electron beam lithography system is first used to define an area with negative photoresist, which is used as the RGB pixel. The green pixels are all shaped into rectangular mesas. The remaining red and blue regions form NR arrays with hexagonal close packing. After that, nickel is deposited by electron beam evaporation, and then the photoresist is removed by a lift-off process to form a hard mask pattern. Subsequently, by using Inductively Coupled Plasma Reactive Ion Etching (ICP-RIE), the GaN-based material is etched to define the active regions, separating the pn layers and isolating each subpixel. Next, residual nickel is removed by HCl solution. The ALD technology was used to deposit the $Al_2O_3$ passivation layer. In order to create color conversion layer, CdSe/ZnS red QDs were sprayed on a region of blue NR-μLED via the super-inkjet (SIJ) printing system. Then, spin-on glass (SOG) was used to isolate the pn electrodes and protect the QD layer. After, a transparent conducting oxide (TCO) layer was orderly deposited via the hole process by SOG etching and Ni/Au metal deposition for the pn electrodes with the lift-off process. Finally, a distributed Bragg reflector (DBR) was used to recycle blue light and cover the red color region to filter out. **Figure 4(b)** showed the SEM image of NR-μLED with 30° tilt angle. Besides, it can be clearly observed from the transmission electron microscopy (TEM) images in **Figure 4(c)** that the sidewalls of MQWs were closely surrounded by QDs, which is important to the NRET mechanisms.

The overlapping relationship between the absorption spectrum of red QDs and the EL spectrum of a blue NR-μLED was demonstrated in **Figure 5(a)**. The emission wavelength of the blue NR-μLED is 467 nm, which is in the range of intense QD absorption. That indicates good spectral overlaps of MQWs with QD absorption and

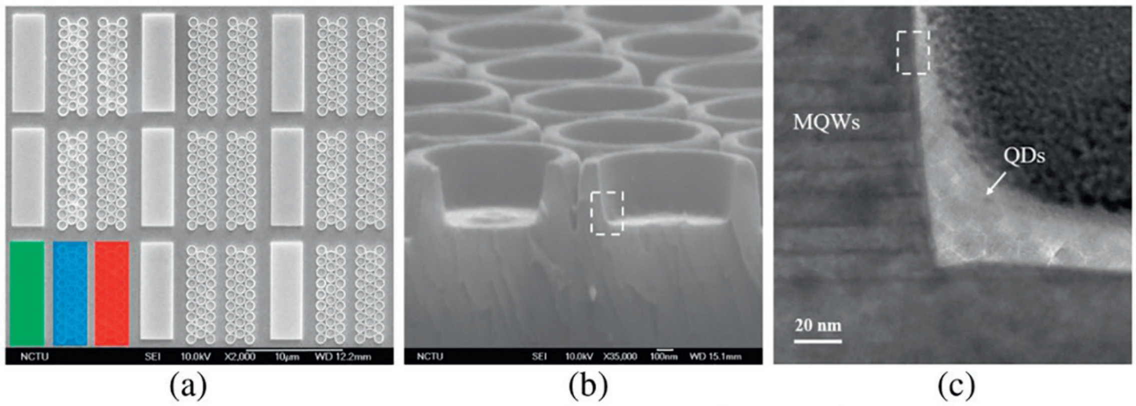


**Figure 4.**
*(a) SEM image of RGB pixel array (top view); (b) SEM image of NR-μLED with 30° tilt angle; (c) TEM image of the contact area between MQWs and QDs [32]. Figures reproduced with permission from Optica Publishing Group.*

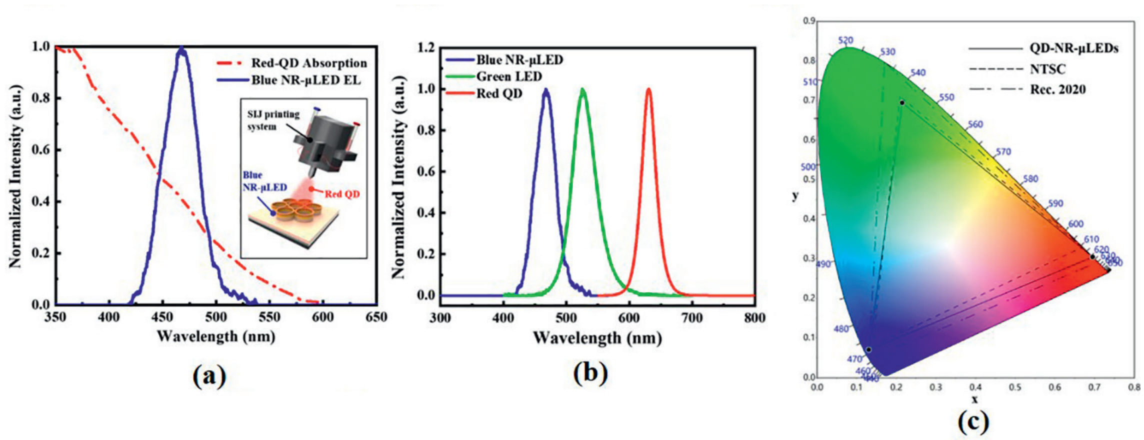


**Figure 5.**
*(a) Absorption curve of red QDs and electroluminescence (EL) spectrum of blue NR-μLEDs (inset depicts a schematic configuration of spraying red QDs on blue NR-μLEDs using the SIJ printing system). (b) EL spectra of RGB hybrid QD-NR-μLEDs; (c) color gamut of RGB hybrid QD-NR-μLEDs, NTSC, and Rec. 2020 [32]. Figures reproduced with permission from Optica Publishing Group.*

makes sure the strong coupling exists between excitons in MQWs and the absorption dipoles of QDs. Moreover, the inset of **Figure 5(a)** schematically shows the process of spraying red QDs on blue NR-μLEDs by using the SIJ printing system. **Figure 5(b)**. demonstrated the EL spectra of individual RGB colors in hybrid QD-NR-μLEDs, the peak wavelengths at 467,525, and 630 nm, respectively. Due to the narrow EL spectra, the fabricated QD-NR-μLEDs can achieve a wide color gamut, which overlaps the NTSC space at approximately 104.8%, and overlaps Rec. 2020 space at about 78.2%.

In recent years, inkjet printing combined with photolithography, namely photolithography-inkjet printing (PHO-IJP) is usually used to fabricate a single pixel of conventional semiconductor quantum dots, with pixel pits on a substrate being created by photolithography followed by filling them with ink via inkjet printing [33]. In 2022, Bai et al. proposed "Interface Engineering-Inkjet Printing-Plasma Etching (IE-IJP-PE)" to fabricate large-area μPeLEDs with microscale and self-emissive pixels [34]. To achieve full-color display, $CsPbCl_{1.56}Br_{1.44}$ (blue), $CsPbBr_3$ (green), and $CsPbBrI_2$ (red) PeQD cyclohexylbenzene solutions were used as RGB inks. The micro-PeLED arrays were constructed with a structure of glass/ITO/PEDOT: PSS/PVK/SDS/RGB PeQD arrays/TPBi/LiF/Al. The fabricated substrates were ultrasonically cleaned sequentially in detergent, acetone, ethanol, and deionized water and dried. After the devices were dried, the ITO glass substrates were treated with UV ozone to remove residual organics for 15 min. The filtered PEDOT:PSS solution with a poly(tetrafluoroethylene) syringe filter (0.45 μm) was spin-coated onto an ITO glass substrate at 4000 rpm for 30 s and annealed at 140°C for 15 min. Dissolve PVK in chlorobenzene to form a 5 mg ml solution. The filtered PVK solution was spin-coated with a 0.45 μm poly(tetrafluoroethylene) syringe filter onto the PEDOT:PSS layer at 3000 rpm for 30 s and annealed at 130°C for 15 min in a glove box. SDS was then spin-coated at 3000 rpm for 30 s and heated at 100°C for 15 min. The RGB PeQD ink was printed on the hole transport layer in air by an IJP process and then treated by plasma cleaning for 15 s to destroy the excess hole transport layer and reduce the leakage current of the micro-PeLED array. Finally, the samples with RGB PeQD arrays were transferred to an interconnected high-vacuum deposition system through thermal evaporation to complete the device. The color gamut of RGB μPeLEDs covers 135% of NTSC, which is much wider than full-color μLEDs fabricated from red and green CdSe-based QDs. In addition, the red μPeLED has a maximum EQE of 0.832%, which is higher than its InGaN-based and AlInGaP-based counterparts.

As mentioned earlier, QD printing technology has become increasingly mature. However, inkjet printing is difficult to achieve large-area production. Colloidal quantum dots exhibit unique optical properties derived from quantum confinement effects that make them suitable for use as color-conversion layers for μLEDs [35]. PRs can be used to combine with quantum dots to form QDPRs after surface modification. By changing the parameters, QDPR can freely control thickness and size, while retaining the advantages of lithography. This method provides a cost-effective and practical solution for the development of large-area, high-resolution fabrication of full-color μLEDs for display applications.

In 2020, Chen et al. demonstrated a full-color μLED display with high color stability using semipolar (20–21) InGaN LEDs and quantum-dot photoresist [36]. To overcome the expensive and not desirable mass production of the conventional way, an innovative orientation-controlled epitaxy (OCE) process with semipolar GaN material selectively grown directly on the standard sapphire wafer was used in this work. The μLED array process started with depositing a transparent conducting oxide (TCO) layer, then, a p-type ohmic contact was formed by annealing at 450°C with the ambient atmospheric conditions. Next, in order to form a 1 μm depth mesa etch and etch the TCO film, inductively coupled plasma-reactive ion etching (ICP-RIE) and an HCl solution were used respectively in this research. Afterward, by using electron beam evaporation, Ti/Al/Ti/Au layers were deposited as the n-type electrode. After that, with the help of plasma-enhanced chemical vapor deposition, a 200 nm thick $SiO_2$ passivation layer was deposited. Eventually, followed by ICP-RIE, the μLED array was completed by the via-hole process. After the μLED array process, as shown in **Figure 6(a)**, the Ni/Au (p-electrode metal) lines were deposited on the flattened surface to link each chip, as shown in **Figure 6(b)**. Then, by using lithography process, the gray photoresist, red QDPR, green QDPR, and transparent PR were fabricated sequentially to form a color pixel on a highly-transparent glass substrate with 0.7 mm thickness, as shown in **Figure 6(c)**. Finally, in **Figure 6(d)**, an aligner and UV resin are used to stick the color pixel array on the glass. The gray PR mold can attain a higher height and provide higher reflectivity, which can reduce the cross-talk effect among pixels and enhance output intensity by inside reflection compared to the

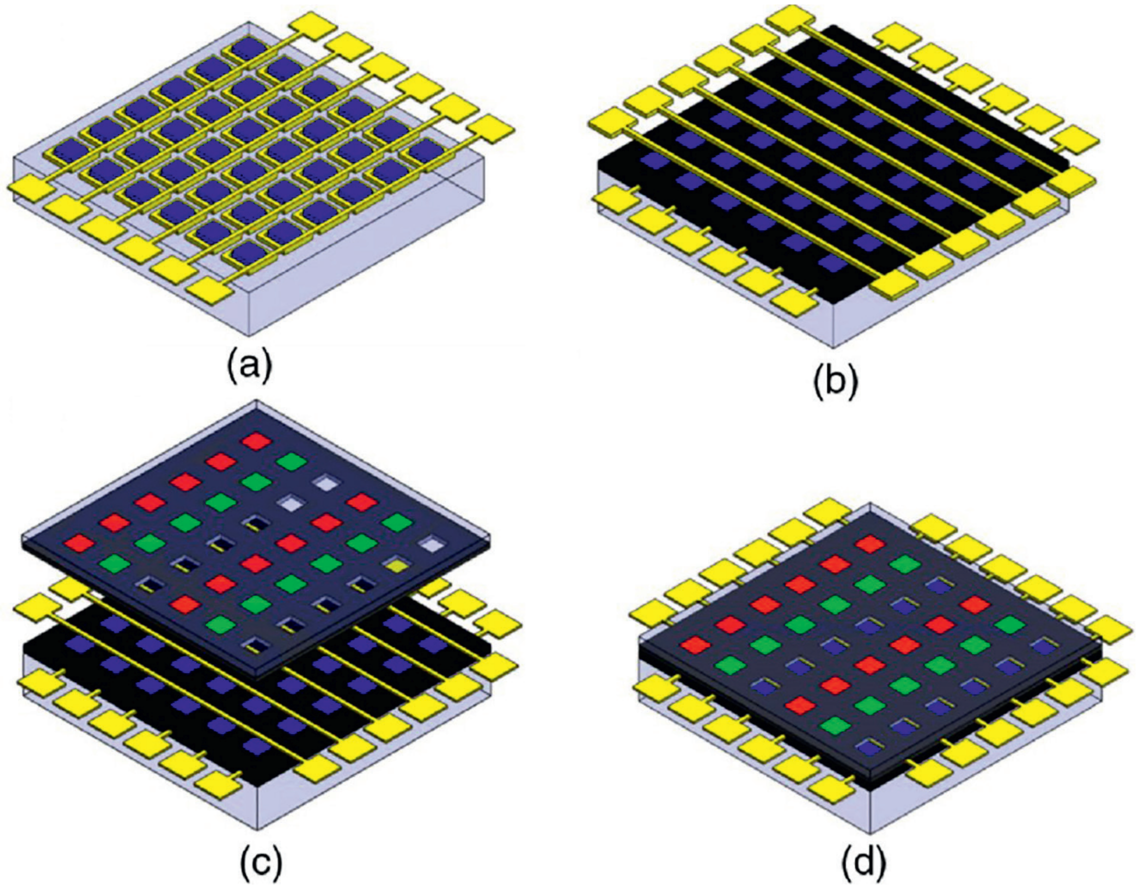


**Figure 6.**
*Process flow for the fabrication of a full-color RGB pixel array. (a) μLED array process. (b) Black PR matrices and p-electrode metal lines. (c) Red, green, and blue (transparent) pixel lithography process. (d) Color pixel bonding [36]. Figures reproduced with permission from Optica Publishing Group.*

black PR. Besides, the semipolar μLED shows a stabilizing wavelength shift of 3.2 nm, while the c-plane μLED's shift is 13.0 nm. Above all, the RGB pixels present a wide color gamut of 114.4% NTSC and 85.4% Rce.2020, showing great promise for display applications. The research also demonstrated a color-conversion layer consisting of QDPR is capable of the common lithography process, which is suitable for large-scale manufacturing.

Recently, μLED all-rounder displays based on silicon backplanes have also attracted the attention of researchers. In 2020, Kawanishi et al. reported a silicon-based full-color micro-LED display, called "Silicon Display" [37]. To fabricate the display array, a p-electrode layer is first formed on the p-GaN layer of the LED epitaxial wafer. The epitaxial layer was then etched down to the n-GaN layer by photolithographic patterning using ICP to form the mesa structure, and the n-GaN layer was exposed to form the n-electrode. Each pixel is defined by a groove down to the sapphire substrate formed by another ICP etch. **Figure 7(a)** shows a schematic diagram of a single pixel. Red and green sub-pixels are formed by exciting the QD color converters with blue LEDs. The quantum dot material is deposited on the surface of the device by a photolithography process after being mixed with a photoresist. A full-color silicon display with a resolution of 1053 ppi and 352 × 198 pixels, each of which is 24 μm in size, is realized. **Figure 7(b)** shows a photo of the overall display. As can be seen from the photo, each QD layer was successfully formed on each sub-pixel through the photolithography process.

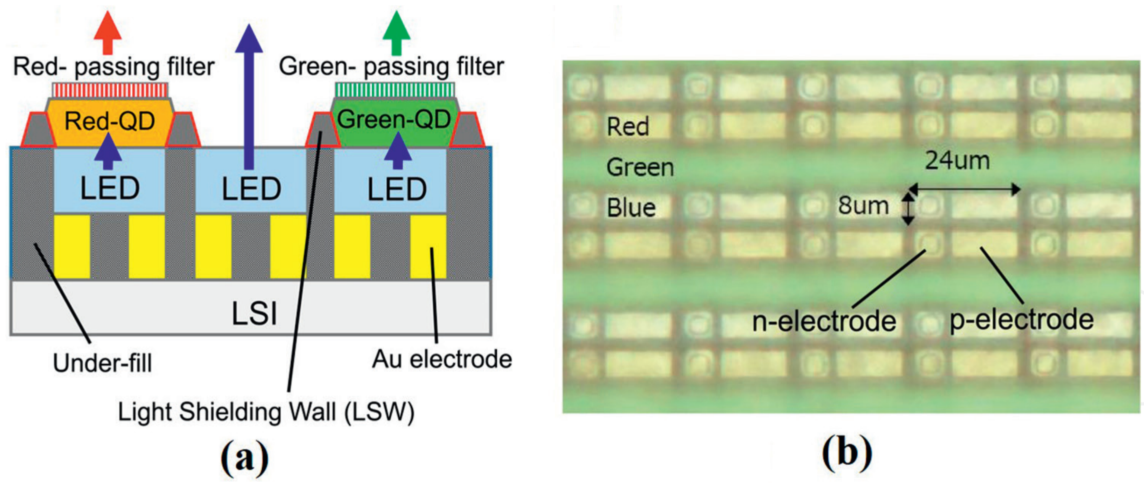


**Figure 7.**
*(a) Schematic cross-section of a single pixel of silicon display. (b) Optical micrograph of 1053 ppi micro-LED array during fabrication after forming red and green QDs [37]. Figures reproduced with permission from the SOCIETY FOR INFORMATION DISPLAY.*

### 2.4 VLC applications with QD-based color-conversion μLEDs

Incorporating a color conversion layer can allow μLEDs to simultaneously achieve full-color display and high-speed modulation. However, the modulation bandwidth of this class of devices is significantly limited by the long response times of color-converting materials [38]. The traditional phosphor material used as the color conversion layer is yttrium aluminum garnet (YAG) phosphor $Y_3$–$xAl_5O_{12}$:$xCe^{3+}$ (YAG:Ce) [39], which has a critical limitation for VLC applications due to the slow phosphor conversion process caused by the long excited-state lifetimes [40], on the order of microseconds. The modulation bandwidth of phosphors is typically only a few MHz [41]. To overcome the bottleneck in response speed, organic materials, such as BODIPY, MEH-PPV and BBEHP-PPV have been recently used as potential candidates for color converters for VLCs due to their visible light emission, high PLQY, direct radiative recombination, and ease of integration with nitride-based semiconductors [42]. However, their excited state lifetimes are still very long. Therefore, developing light-converter phosphor materials with fast decay and high efficiency (that is, short radiative lifetime and high brightness) remains a major challenge for VLC and solid-state lighting (SSL) applications.

As previously introduced, quantum dot (QD)-based color converters have very promising applications, however, the modulation bandwidth of conventional CdSe/ZnS QDs is limited to ~3 MHz, which is much lower than the requirement of VLC [43]. Lead halide perovskite QDs exhibit high PLQY (≥70%) and relatively short PL lifetimes [27]. In 2018, Shi et al. reported an all-inorganic white light system for VLC [44]. The system uses blue GaN-based μLEDs as the excitation light source and inorganic yellow-emitting $CsPbBr_{1.8}I_{1.2}$ perovskite quantum dots (YQDs) as the color conversion layer. The maximum modulation bandwidth of the packaged 80 μm × 80 μm blue-emitting μLED is about 160 MHz, and the peak emission wavelength is about 445 nm. Maximum −3 dB E-O modulation bandwidths of ~73 and ~85 MHz were achieved for perovskite quantum dots and white light systems combining μLED and perovskite quantum dots, respectively. In addition, based on the high bandwidth white light system, the real-time data rate is 300 Mbps using no return Zero-On–Off Keying (NRZ-OOK) modulation scheme.

Most GaN-based μLEDs are typically grown on (0001) "polar" c-plane sapphire substrates, which leads to strong Stark effect QCSE effect (QCSE), which, in addition to leading to a drop in efficiency, will limit the modulation bandwidth of μLEDs [45]. The spontaneous polarization of GaN is responsible for the QCSE due to the highest symmetry compatible with its structure. Meanwhile, the strain caused by the lattice mismatch between InxGa1 − xN and GaN also produces polarization. These internal polarization fields along the c-plane will lead to band tilting, separating the wave functions of electrons and holes. QCSE also causes wavelength shift and efficiency drop with increasing injection current density. The applications of the semipolar (20–21) and (20–2–1) epitaxial structures have been proven to effectively suppress the effects of QCSE [46]. Semipolar devices enable higher modulation bandwidths due to weak polarization fields and flat energy gap distributions, which lead to larger electron–hole wavefunction overlap reducing carrier lifetimes [47]. Further, Zhao et al. revealed that faster carrier transport in semipolar devices also contributes to the weaker phase-space filling effect, which was determined for the low-droop phenomenon in semipolar LEDs because of small QCSE and short carrier lifetimes using the consistency between theoretical and experimental results [48]. The aforementioned advantages imply that a semipolar LED is capable of simultaneously achieving high modulation speed and maintaining high efficiency with increasing injected current owing to low droop performance.

In 2020, Huang Chen et al. realized long-wavelength (initial wavelength 540 nm) InGaN/GaN VLC-LEDs with high 3 dB bandwidth using semipolar epitaxy and μLED structures [49]. The epitaxial process of semipolar (20–21) GaN on a (22–43) PSS is carried out through a low-pressure metalorganic chemical vapor deposition (MOCVD). In addition, the passivation layer of aluminum oxide ($Al_2O_3$) was grown to repair sidewall defects. Some previous studies have stated that the influence of sidewall defects increases as the chip size decreases [50, 51]. In particular, when the LED device achieves a micrometer scale, traditional passivation methods, such as the PECVD process, are no longer useful owing to the large leakage current of the μLED device. ALD dielectric thin films have been regarded as an effective passivation technique in the μLED area [52]. The semipolar device had a shorter lifetime because of the weak polarization-related electric field and large overlap of the electron–hole wave function, which yielded a faster carrier recombination lifetime [53]. The QCSE reduction in the semipolar device yielded faster carrier transport and a shorter recombination lifetime, resulting in a weaker phase-space filling effect. Therefore, the semipolar μLED can achieve a high modulation bandwidth owing to its faster carrier recombination lifetime.

The outstanding performance of semipolar μLEDs in display and communication has also led researchers to combine it with QDs to make high-performance full-color display devices with VLC potential. In 2021, Singh et al. proposed a flexible white-light system for high-speed VLC applications [54]. The white-light system fabrication process is shown in **Figure 8**. The system consists of nanostructured green $CsPbBr_3$ PQD paper, red CdSe QD paper, and semipolar blue micro-LEDs. Regarding the production of green $CsPbBr_3$ PQD paper, firstly, a solution of $CsPbBr_3$ quantum dots were prepared using the hot injection method, and then the solution was added to the cellulose nanocrystal (CNC) suspension, and the mixed solution was filtered through a filter membrane using a vacuum pump device. The PQD paper in nanostructured form is then separated from the filter membrane. The QD paper produced by this method has strong mechanical strength and flexibility to be used with flexible systems. In addition, the PQD paper fabricated by this method has nanostructures, which should provide a strong quantum confinement effect to increase

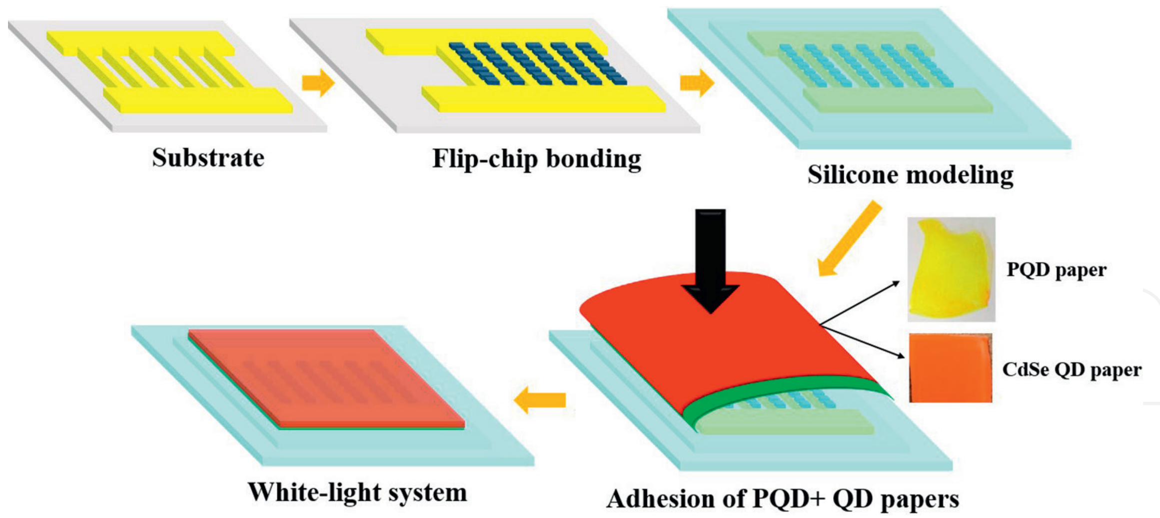


**Figure 8.**
*Fabrication of white-light system [54]. Figures reproduced with permission from Optica Publishing Group.*

the probability of carrier recombination. The flexible μLED was fabricated using a polyimide (PI) substrate covered with copper-foil shielding tape, where the latter was subjected to photolithography and wet etching to establish electrical conduction. The μLED flip-chip was bonded on the PI substrate using a silicone-based electrically conductive anisotropic adhesive to maintain the electrical conductivity between the chip metal contact and the AuSn solder on the substrate; this increased the system flexibility. For the color converter, $CsPbBr_3$ PQD paper and CdSe QD paper were prepared. These papers were adhered to the top of the μLED with flexible substrate using an adhesive to achieve white-light system.

Semipolar μLEDs had a narrow FWHM and was therefore responsible for the delivery of pure emitted light, matching colors, and a wide color gamut. **Figure 9(a)** shows the color performance of the white-light system created using the semipolar blue μLED with PQD paper and CdSe QD paper under driving conditions from 10 to 1200 $A/cm^2$. The white-light system demonstrated a wide color gamut, achieving 98.7% of the NTSC and 91.1% Rec. 2020 of the CIE 1931. The color gamut of the white-light system remained almost unchanged with increasing injection current density owing to the wavelength stability.

The average PL lifetimes calculated for the PQD paper and CdSe QD paper were 5.92, and 12.88 ns, as shown in **Figure 9(b)**. The PQD paper had a shorter carrier lifetime than those reported in other studies, while also being considerably shorter than those of phosphors microsecond to millisecond range. This shorter carrier lifetime is attributable to the quantum confinement effect, which yields faster radiative recombination. However, the CdSe QD-paper carrier recombination lifetime is insufficient to independently achieve high bandwidth for VLC applications. Therefore, semipolar μLEDs and PQDs have considerable potential for VLC applications. The PQD-film bandwidth was found to be 111 MHz, as shown in **Figure 9(c)**; the PQD-based white-light system also displayed a frequency bandwidth of 95.5 MHz at a 113 mA injection current. Hence, the high bandwidth of the PQD paper is suitable for achieving high-speed VLC. This outcome implies that the nanostructure has a higher recombination rate than the bulk and hence a higher modulation bandwidth.

Although PQDs have significant advantages over traditional color conversion materials, they also have some drawbacks. They have, for example, exhibited vulnerability under ambient conditions, particularly in the case of red-emitting PQDs that

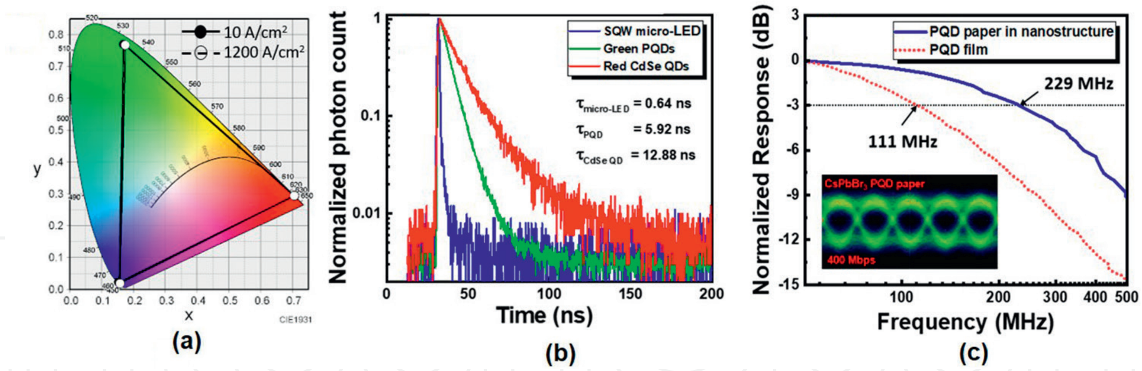


**Figure 9.**
*(a) Color gamut of white-light system according to CIE 1931 color space under various current densities. (b) TRPL curves for semipolar µLED and PQD and CdSe QD papers. (c) Comparison of bandwidth of PQD paper in nanostructure with that of PQD film, Inset: eye diagram for PQD paper [54]. Figures reproduced with permission from Optica Publishing Group.*

contain iodine [55]. The application bottleneck of PQDs is long-term stability. It degrades rapidly when exposed to the environment. Water vapor, oxygen, high temperature, and light irradiation cause alteration to the crystal structures of PQDs, typically resulting in photoluminescence (PL) quenching [56]. These four factors coexist in the environment, so their effects are difficult to distinguish from each other [57]. In terms of immediate optical performance, most of the crystal structure changes are negative, but a few of them are positive. Therefore, the high-stability PQDs color conversion layer made by the new encapsulation method will have good application prospects in the fields of display and communication. Embedding QDs in organic polymers can significantly extend their lifetimes, as the polymers ensure a hermetic seal from air [58, 59]. In the current study, the organic shell is still not perfect because the polymer cannot withstand UV or blue illumination from the excitation light source for long periods of time [60]. Thus, shells composed of inorganic substances have been favored since recently, including $Al_2O_3$, $ZrO_2$, and anodized aluminum templates [61, 62]. Although these inorganic shells can withstand blue light and UV irradiation better than organic shells, the porous structures are not as water/$O_2$-proof as the organic ones because the pore structures remain. In 2021, Lin et al. reported an inorganic encapsulation of mesoporous $SiO_2$, in conjunction with a high-temperature sintering synthesis process under an inert atmosphere [58]. This synthesis process is compatible with various halide contents, yielding PeNCs sealed in $SiO_2$ particles that emit PL emission covering the entire visible range from 420 to 700 nm. The PeNCs–$SiO_2$ sample showed remarkable stability after undergoing aging tests under various exaggerated stresses as well as mitigated thermal quenching during thermal cycling. The PeNCs–$SiO_2$ can be blended into a photoresist and remains luminous during the development procedure, which is compatible with the photolithography process; this facilitates the mass production of color conversion layers. This robust encapsulation also has great application value for full-color display or visible light communication based on quantum dot-based µLED.

In 2021, Wu et al. reported a PNC–µLED device for a full-color display that is developed using a semipolar (20–21) blue µLED array with green-emitting $CsPbBr_3$ and red-emitting $CsPbBrI_2$ PNCs [63]. They encapsulated the PQDs in an all-inorganic $SiO_2$ shell, which significantly improved the stability of the color conversion layer. Regarding the fabrication of $CsPbBrI_2$-$SiO_2$, the precursor solution was first prepared by mixing the precursor salt with MCM-41 molecular sieves and dispersing the mixture in 25 ml of purified water. Next, the precursor solution was sonicated for 20 min and vigorously stirred for 10 min to improve dispersion. The precursor solution was transferred into a crucible and placed in a tube furnace filled with high-purity Ar gas. The temperature of the tube furnace was raised to 200°C and kept for 1 h to evaporate the water. Then, sintering was performed continuously for 30 min at a temperature of 750°C with an Ar flow rate of 15 ml/min. Subsequently, the samples were cooled to room temperature under Ar protection, during which their color gradually changed and finally crystallized into PNCs. During cooling, the perovskite forms inside the $SiO_2$, which constrains the PNCs inside that facilitate the formation of crystal phase, thereby ensuring the high stability of the red-emitting PNCs. **Figure 10(a)** illustrates

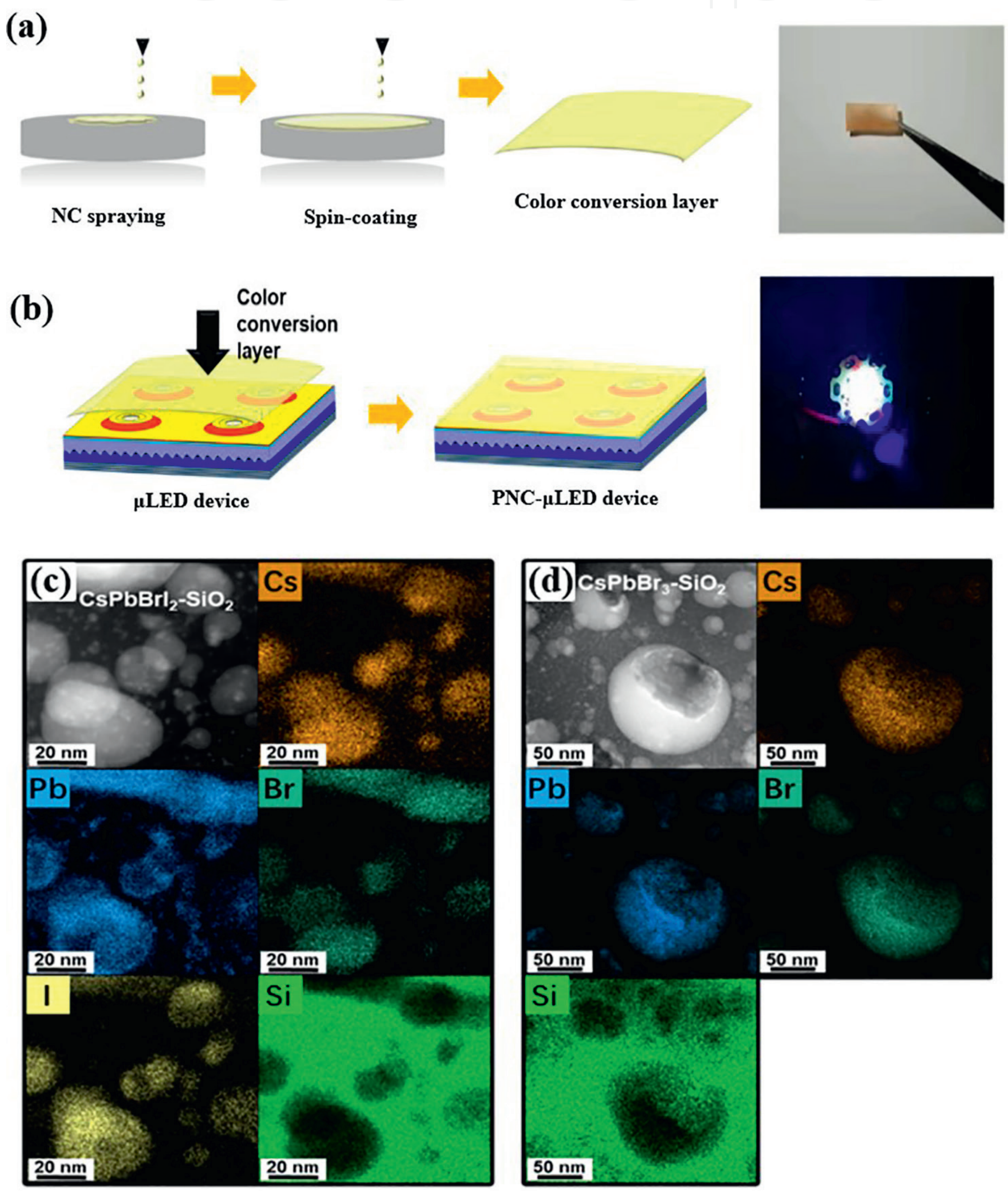


**Figure 10.**
*(a) The fabrication process and a photo of the color conversion layer; and (b) the proposed PNC-µLED device. EDS element maps of the (a) $CsPbBrI_2$-$SiO_2$ and (b) $CsPbBr_3$-$SiO_2$ PNCs [63]. Figures reproduced with permission from Optica Publishing Group.*

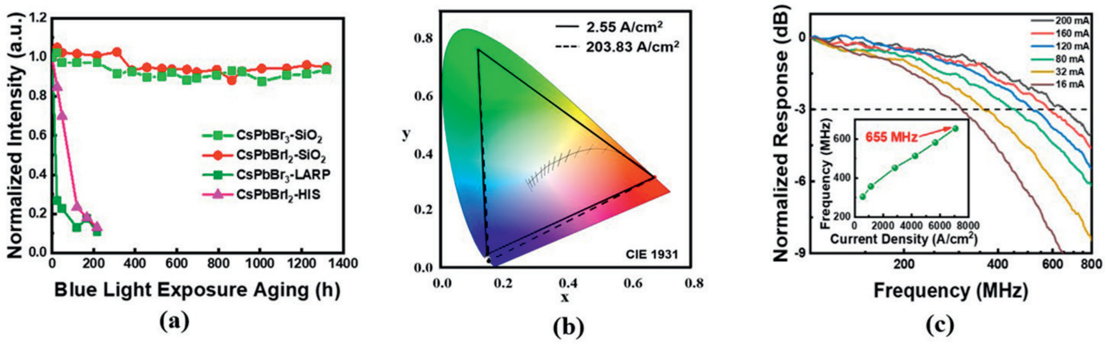


**Figure 11.**
*(a) The normalized intensity of the PL properties of the red and green PNCs, as well as the solution-processed samples under blue light exposure. (b) Color gamut of the PNC-μLED under different current densities. (c) Frequency response for the PNC-μLED [63]. Figures reproduced with permission from Optica Publishing Group.*

the fabrication detail and presents a photo of the as-fabricated films under natural light, which are composed of $CsPbBr_3$-$SiO_2$ and $CsPbBrI_2$-$SiO_2$. During this process, $CsPbBrI_2$-$SiO_2$ and $CsPbBr_3$-$SiO_2$ were mixed with toluene to make a red and green mixture. The EVA polymer was dissolved into the mixture and heated to 50°C with stirring. The mixture was then spin-coated (1800 rad/s) on a glass substrate to obtain a thin film of uniform thickness. In **Figure 10(b)**, the color conversion layer is combined with the semipolar μLED, achieving the white-light PNC-μLED device for the backlight. The fine structure of both PNC samples is also revealed from the EDS element maps, as illustrated in **Figure 10(c)** and **(d)**. These maps indicate that the spatial distribution of the elements within the PNCs is highly similar; they are confined to approximately circular regions surrounded by areas of $SiO_2$. This further confirms the encapsulation of the PNCs inside $SiO_2$ shells.

**Figure 11(a)** shows the normalized intensity of the PL properties of the red and green PNCs, as well as the solution-processed samples under blue light exposure. The $SiO_2$-embedded samples exhibit remarkable stabilities, showing no degradation under blue irradiation. **Figure 11(b)** shows the frequency response of the PNC-μLED, the highest 3-dB bandwidth was measured as 655 MHz, corresponding to an injection current of 200 mA. **Figure 11(c)** presents the performance of the PNC-μLED for the display backlight application under different current densities between 2.55 and 203.83 $A/cm^2$. Because of its narrow EL spectrum, the RGB pixel assembled from the semipolar μLEDs and PNCs exhibited a wide color gamut of 127.23% of the NTSC and 95.00% of the Rec. 2020.

## 3. Conclusions

QDs-based μLED provide superior display performance and are a promising platform for VLC systems. In this article, we comprehensively review recent progress in QD-based μLED devices. It includes the research status of various QDs and white LEDs based on QDs color conversion layers. The fabrication of QD-based high-resolution full-color μLEDs is also discussed. Including charge-assisted layer-by-layer (LbL), aerosol jet printing, and super inkjet printing methods to fabricate QD-based μLEDs. The use of quantum dot photoresist in combination with semipolar μLEDs is also described. Finally, we discuss the research of QD-based μLEDs for visible light communication, which allows a single device to be used for both display and high-speed communication, enhancing the versatility of μLEDs. Advances in the development of QD-based μLEDs are expected to make this display technology ubiquitous in the near future. Recent breakthroughs in QDs and LEDs will provide a promising outlook for future demand in the semiconductor industry.

## Acknowledgements

Additionally, we thank Xiangshu Lin for their contributions to the investigation.

## Funding

This research was supported by the National Natural Science Foundation of China (62274138, 11904302), Science and Technology Plan Project in Fujian Province of China (2021H0011), Major Science and Technology Project of Xiamen, China (3502Z20191015).

## Author details

Tingzhu Wu[1,2], Tingwei Lu[1], Yen-Wei Yeh[3], Zhong Chen[1,2] and Hao-Chung Kuo[3,4]*

1 School of Electronic Science and Engineering, Fujian Engineering Research Center for Solid-State Lighting, Xiamen University, Xiamen, China

2 Innovation Laboratory for Sciences and Technologies of Energy Materials of Fujian Province (IKKEM), Xiamen, China

3 Department of Photonics, Graduate Institute of Electro-Optical Engineering, College of Electrical and Computer Engineering, National Yang Ming Chiao Tung University, Hsinchu, Taiwan

4 Semiconductor Research Center, Hon Hai Research Institute, Taipei, Taiwan

*Address all correspondence to: hckuo@faculty.nctu.edu.tw

## References

[1] Alivisatos P. The use of nanocrystals in biological detection. Nature Biotechnology. 2004;**22**(1):47-52. DOI: 10.1038/nbt927

[2] Tian PF, McKendry JJD, Gu ED, Chen ZZ, Sun YJ, Zhang GY, et al. Fabrication, characterization and applications of flexible vertical InGaN micro-light emitting diode arrays. Optics Express. 2016;**24**(1):699-707. DOI: 10.1364/oe.24.000699

[3] Liu ZJ, Zhang K, Liu YB, Yan SW, Kwok HS, Deen J, et al., editors. Fully multi-functional GaN-based micro-LEDs for 2500 PPI micro-displays, temperature sensing, light energy harvesting, and light detection. In: 64th IEEE Annual International Electron Devices Meeting (IEDM); December 01-05, 2018. New York, San Francisco, CA: IEEE; 2018

[4] Singh KJ, Huang YM, Ahmed T, Liu AC, Chen SWH, Liou FJ, et al. Micro-LED as a promising candidate for high-speed visible light communication. Applied Sciences—Basel. 2020;**10**(20):7384. DOI: 10.3390/app10207384

[5] Khan LU. Visible light communication: Applications, architecture, standardization and research challenges. Digital Communications and Networks. 2017;**3**(2):78-88. DOI: 10.1016/j.dcan.2016.07.004

[6] Chow CW, Yeh CH, Liu YF, Liu Y. Improved modulation speed of LED visible light communication system integrated to main electricity network. Electronics Letters. 2011;**47**(15):867-U1954. DOI: 10.1049/el.2011.0422

[7] Cho J, Park JH, Kim JK, Schubert EF. White light-emitting diodes: History, progress, and future. Laser & Photonics Reviews. 2017;**11**(2):1600147. DOI: 10.1002/lpor.201600147

[8] Bulashevich KA, Karpov SY. Impact of surface recombination on efficiency of III-nitride light-emitting diodes. Physica Status Solidi-Rapid Research Letters. 2016;**10**(6):480-484. DOI: 10.1002/pssr.201600059

[9] Hwang D, Mughal A, Pynn CD, Nakamura S, DenBaars SP. Sustained high external quantum efficiency in ultrasmall blue III-nitride micro-LEDs. Applied Physics Express. 2017;**10**(3):032101. DOI: 10.7567/apex.10.032101

[10] Wang XC, Bao Z, Chang YC, Liu RS. Perovskite quantum dots for application in high color gamut backlighting display of light-emitting diodes. ACS Energy Letters. 2020;**5**(11):3374-3396. DOI: 10.1021/acsenergylett.0c01860

[11] Lin CH, Verma A, Kang CY, Pai YM, Chen TY, Yang JJ, et al. Hybrid-type white LEDs based on inorganic halide perovskite QDs: Candidates for wide color gamut display backlights. Photonics Research. 2019;**7**(5):579-585. DOI: 10.1364/prj.7.000579

[12] Lin CC, Liu RS. Advances in phosphors for light-emitting diodes. Journal of Physical Chemistry Letters. 2011;**2**(11):1268-1277. DOI: 10.1021/jz2002452

[13] Huang YM, Singh KJ, Hsieh TH, Langpoklakpam C, Lee TY, Lin CC, et al. Gateway towards recent developments in quantum dot-based light-emitting diodes. Nanoscale. 2022;**14**(11):4042-4064. DOI: 10.1039/d1nr05288h

[14] Sapsford KE, Pons T, Medintz IL, Mattoussi H. Biosensing

with luminescent semiconductor quantum dots. Sensors. 2006;**6**(8):925-953. DOI: 10.3390/s6080925

[15] Araki Y, Ohkuno K, Furukawa T, Saraie J. Green light emitting diodes with CdSe quantum dots. Journal of Crystal Growth. 2007;**301**:809-811. DOI: 10.1016/j.jcrysgro.2006.11.105

[16] Du JH, Wang CL, Xu XJ, Wang ZY, Xu SH, Cui YP. Assembly of light-emitting diode based on hydrophilic CdTe quantum dots incorporating dehydrated silica gel. Luminescence. 2016;**31**(2):419-422. DOI: 10.1002/bio.2976

[17] Morris-Cohen AJ, Donakowski MD, Knowles KE, Weiss EA. The effect of a common purification procedure on the chemical composition of the surfaces of CdSe quantum dots synthesized with Trioctylphosphine oxide. Journal of Physical Chemistry C. 2010;**114**(2):897-906. DOI: 10.1021/jp909492w

[18] Stan CS, Secula MS, Sibiescu D. Highly luminescent polystyrene embedded CdSe quantum dots obtained through a modified colloidal synthesis route. Electronic Materials Letters. 2012;**8**(3):275-281. DOI: 10.1007/s13391-012-1108-0

[19] Soheyli E, Ghaemi B, Sahraei R, Sabzevari Z, Kharrazi S, Amani A. Colloidal synthesis of tunably luminescent AgInS-based/ZnS core/shell quantum dots as biocompatible nano-probe for high-contrast fluorescence bioimaging. Materials Science & Engineering C-Materials for Biological Applications. 2020;**111**:110807. DOI: 10.1016/j.msec.2020.110807

[20] Reifsnyder DC, Ye XC, Gordon TR, Song CY, Murray CB. Three-dimensional self-assembly of chalcopyrite copper indium Diselenide nanocrystals into oriented films. ACS Nano. 2013;**7**(5):4307-4315. DOI: 10.1021/nn4008059

[21] Chen B, Li DY, Wang F. InP quantum dots: Synthesis and lighting applications. Small. 2020;**16**(32):2002454. DOI: 10.1002/smll.202002454

[22] Brus LE. Electron electron and electron-hole interactions in small semiconductor crystallites—The size dependence of the lowest excited electronic state. Journal of Chemical Physics. 1984;**80**(9):4403-4409. DOI: 10.1063/1.447218

[23] Chen O, Wei H, Maurice A, Bawendi M, Reiss P. Pure colors from core-shell quantum dots. MRS Bulletin. 2013;**38**(9):696-702. DOI: 10.1557/mrs.2013.179

[24] Zhang ZL, Liu D, Li DZ, Huang KK, Zhang Y, Shi Z, et al. Dual emissive Cu:InP/ZnS/InP/ZnS nanocrystals: Single-source "greener" emitters with flexibly Tunable emission from visible to near-infrared and their application in white light-emitting diodes. Chemistry of Materials. 2015;**27**(4):1405-1411. DOI: 10.1021/cm5047269

[25] Milstein TJ, Kroupa DM, Gamelin DR. Picosecond quantum cutting generates photoluminescence quantum yields over 100% in ytterbium-doped CsPbCl3 nanocrystals. Nano Letters. 2018;**18**(6):3792-3799. DOI: 10.1021/acs.nanolett.8b01066

[26] Schmidt LC, Pertegas A, Gonzalez-Carrero S, Malinkiewicz O, Agouram S, Espallargas GM, et al. Nontemplate synthesis of CH3NH3PbBr3 perovskite nanoparticles. Journal of the American Chemical Society. 2014;**136**(3):850-853. DOI: 10.1021/ja4109209

[27] Protesescu L, Yakunin S, Bodnarchuk MI, Krieg F, Caputo R, Hendon CH, et al. Nanocrystals of cesium Lead halide perovskites (CsPbX3, X = Cl, Br, and I): Novel optoelectronic materials showing bright emission with wide color gamut. Nano Letters. 2015;**15**(6):3692-3696. DOI: 10.1021/nl5048779

[28] Wang HC, Bao Z, Tsai HY, Tang AC, Liu RS. Perovskite quantum dots and their application in light-emitting diodes. Small. 2018;**14**(1):1702433. DOI: 10.1002/smll.201702433

[29] Kong CY, Lin CH, Lin CH, Li TY, Chen SWH, Tsai CL, et al. Highly efficient and stable white light-emitting diodes using perovskite quantum dot paper. Advanced. Science. 2019;**6**(24):1902230. DOI: 10.1002/advs.201902230

[30] Han HV, Lin HY, Lin CC, Chong WC, Li JR, Chen KJ, et al. Resonant-enhanced full-color emission of quantum-dot-based micro LED display technology. Optics Express. 2015;**23**(25):32504-32515. DOI: 10.1364/oe.23.032504

[31] Lin HY, Sher CW, Hsieh DH, Chen XY, Chen HMP, Chen TM, et al. Optical cross-talk reduction in a quantum-dot-based full-color micro-light-emitting-diode display by a lithographic-fabricated photoresist mold. Photonics Research. 2017;**5**(5):411-416. DOI: 10.1364/prj.5.000411

[32] Chen SWH, Shen CC, Wu TZ, Liao ZY, Chen LF, Zhou JR, et al. Full-color monolithic hybrid quantum dot nanoring micro light-emitting diodes with improved efficiency using atomic layer deposition and nonradiative resonant energy transfer. Photonics Research. 2019;**7**(4):416-422. DOI: 10.1364/prj.7.000416

[33] Xuan TT, Shi SC, Wang L, Kuo HC, Xie RJ. Inkjet-printed quantum dot color conversion films for high-resolution and full-color micro light-emitting diode displays. Journal of Physical Chemistry Letters. 2020;**11**(13):5184-5191. DOI: 10.1021/acs.jpclett.0c01451

[34] Bai WH, Xuan TT, Zhao HY, Shi SC, Zhang XY, Zhou TL, et al. Microscale perovskite quantum dot light-emitting diodes (micro-PeLEDs) for full-color displays. Advanced Optical Materials. 2022;**10**(12):2200087 DOI: 10.1002/adom.202200087

[35] Erdem T, Demir HV. Color science of nanocrystal quantum dots for lighting and displays. Nano. 2013;**2**(1):57-81. DOI: 10.1515/nanoph-2012-0031

[36] Chen SWH, Huang YM, Singh KJ, Hsu YC, Liou FY, Song J, et al. Full-color micro-LED display with high color stability using semipolar (20-21) InGaN LEDs and quantum-dot photoresist. Photonics Research. 2020;**8**(5):630-636. DOI: 10.1364/prj.388958

[37] Kawanishi H, Onuma H, Maegawa M, Kurisu T, Ono T, Akase S, et al. High-resolution and high-brightness full-colour "silicon display" for augmented and mixed reality. Journal of the Society for Information Display. 2021;**29**(1):57-67. DOI: 10.1002/jsid.968

[38] Xu Y, Chen J, Zhang H, Wei H, Zhou L, Wang Z, et al. White-light-emitting flexible display devices based on double network hydrogels crosslinked by YAG:Ce phosphors. Journal of Materials Chemistry C. 2020;**8**(1):247-252. DOI: 10.1039/C9TC05311E

[39] Li PP, Lu Y, Duan YM, Xu SQ, Zhang JJ. Potential application of perovskite glass material in photocatalysis field. Journal of Physical Chemistry C. 2021;**125**(4):2382-2392. DOI: 10.1021/acs.jpcc.0c11241

[40] Wang ZM, Wei ZX, Cai YT, Wang L, Li MT, Liu P, et al. Encapsulation-enabled

perovskite-PMMA films combining a Micro-LED for high-speed white-light communication. ACS Applied Materials & Interfaces. 2021;**13**(45):54143-54151. DOI: 10.1021/acsami.1c15873

[41] Gao H, Xie YY, Geng C, Xu S, Bi WG. Efficiency enhancement of quantum-dot-converted LEDs by 0D-2D hybrid scatterers. ACS Photonics. 2020;**7**(12):5430-5439. DOI: 10.1021/acsphotonics.0c01240

[42] Su CY, Wu YC, Cheng CH, Wang WC, Wang HY, Chen LY, et al. Color-converting violet laser diode with an ultrafast BEHP-PPV. ACS Applied Electronic Materials. 2020;**2**(9):3017-3027. DOI: 10.1021/acsaelm.0c00619

[43] Xiao X, Tang H, Zhang T, Chen W, Chen W, Wu D, et al. Improving the modulation bandwidth of LED by CdSe/ZnS quantum dots for visible light communication. Optics Express. 2016;**24**(19):21577-21586. DOI: 10.1364/OE.24.021577

[44] Mei SL, Liu XY, Zhang WL, Liu R, Zheng LR, Guo RQ, et al. High-bandwidth white-light system combining a micro-LED with perovskite quantum dots for visible light communication. ACS Applied Materials & Interfaces. 2018;**10**(6):5641-5648. DOI: 10.1021/acsami.7b17810

[45] Piprek J. Efficiency droop in nitride-based light-emitting diodes. Physica Status Solidi A—Applications and Materials Science. 2010;**207**(10):2217-2225. DOI: 10.1002/pssa.201026149

[46] Liu SG, Han SC, Xu CC, Xu HW, Wang XY, Wang D, et al. Enhanced photoelectric performance of GaN-based Micro-LEDs by ion implantation. Optical Materials. 2021;**121**:111579. DOI: 10.1016/j.optmat.2021.111579

[47] Zhao YJ, Fu HQ, Wang GT, Nakamura S. Toward ultimate efficiency: Progress and prospects on planar and 3D nanostructured nonpolar and semipolar InGaN light-emitting diodes. Advances in Optics and Photonics. 2018;**10**(1):246-308. DOI: 10.1364/aop.10.000246

[48] Fu HQ, Lu ZJ, Zhao XH, Zhang YH, DenBaars SP, Nakamura S, et al. Study of low-efficiency droop in semipolar (20(2)over-bar(1)over-bar) InGaN light-emitting diodes by time-resolved photoluminescence. Journal of Display Technology. 2016;**12**(7):736-741. DOI: 10.1109/jdt.2016.2521618

[49] Chen S-WH, Huang Y-M, Chang Y-H, Lin Y, Liou F-J, Hsu Y-C, et al. High-bandwidth green semipolar (20-21) InGaN/GaN micro light-emitting diodes for visible light communication. ACS Photonics. 2020;**7**(8):2228-2235. DOI: 10.1021/acsphotonics.0c00764

[50] Kou JQ, Shen CC, Shao H, Che JM, Hou X, Chu CS, et al. Impact of the surface recombination on InGaN/GaN-based blue micro-light emitting diodes. Optics Express. 2019;**27**(12):A643-AA53. DOI: 10.1364/oe.27.00a643

[51] Yang W, Zhang SL, McKendry JJD, Herrnsdorf J, Tian PF, Gong Z, et al. Size-dependent capacitance study on InGaN-based micro-light-emitting diodes. Journal of Applied Physics. 2014;**116**(4):044512. DOI: 10.1063/1.4891233

[52] Wong MS, Hwang D, Alhassan AI, Lee C, Ley R, Nakamura S, et al. High efficiency of III-nitride micro-light-emitting diodes by sidewall passivation using atomic layer deposition. Optics Express. 2018;**26**(16):21324-21331. DOI: 10.1364/oe.26.021324

[53] Monavarian M, Rashidi A, Aragon A, Oh SH, Nami M, Denbaars SP, et al.

Explanation of low efficiency droop in semipolar (20(21)over-bar) InGaN/GaN LEDs through evaluation of carrier recombination coefficients. Optics Express. 2017;**25**(16):19343-19353. DOI: 10.1364/oe.25.019343

[54] Singh KJ, Fan XT, Sadhu AS, Lin CH, Liou FJ, Wu TZ, et al. CsPbBr3 perovskite quantum-dot paper exhibiting a highest 3 dB bandwidth and realizing a flexible white-light system for visible-light communication. Photonics Research. 2021;**9**(12):2341-2350. DOI: 10.1364/prj.434270

[55] Wei Y, Cheng Z, Lin J. An overview on enhancing the stability of lead halide perovskite quantum dots and their applications in phosphor-converted LEDs. Chemical Society Reviews. 2019;**48**(1):310-350. DOI: 10.1039/C8CS00740C

[56] Shangguan ZB, Zheng X, Zhang J, Lin WS, Guo WJ, Li C, et al. The stability of metal halide perovskite nanocrystals—A key issue for the application on quantum-dot-based micro light-emitting diodes display. Nanomaterials. 2020;**10**(7):1375. DOI: 10.3390/nano10071375

[57] Zhang L, Ju MG, Liang WZ. The effect of moisture on the structures and properties of lead halide perovskites: A first-principles theoretical investigation. Physical Chemistry Chemical Physics. 2016;**18**(33):23174-23183. DOI: 10.1039/c6cp01994c

[58] Lin Y, Zheng X, Shangguan Z, Chen G, Huang W, Guo W, et al. All-inorganic encapsulation for remarkably stable cesium lead halide perovskite nanocrystals: Toward full-color display applications. Journal of Materials Chemistry C. 2021;**9**(36):12303-12313. DOI: 10.1039/D1TC02685B

[59] Liu LG, Deng LG, Huang S, Zhang P, Linnros J, Zhong HZ, et al. Photodegradation of organometal hybrid perovskite nanocrystals: Clarifying the role of oxygen by single-dot photoluminescence. Journal of Physical Chemistry Letters. 2019;**10**(4):864-869. DOI: 10.1021/acs.jpclett.9b00143

[60] Zhang Y, Cai GF, Fang Y, Han GJ. Relaying transmission for multiresolution M-DCSK modulation in multi-relay networks. In: 4th International Conference on Communication and Information Systems (ICCIS); 2019 December 21-23. Wuhan. New York: IEEE; 2019. p. 1-6

[61] Quan LN, Rand BP, Friend RH, Mhaisalkar SG, Lee TW, Sargent EH. Perovskites for next-generation optical sources. Chemical Reviews. 2019;**119**(12):7444-7477. DOI: 10.1021/acs.chemrev.9b00107

[62] Rajagopal A, Yao K, Jen AKY. Toward perovskite solar cell commercialization: A perspective and research roadmap based on interfacial engineering. Advanced Materials. 2018;**30**(32):1800455. DOI: 10.1002/adma.201800455

[63] Wu T, Lin Y, Huang Y-M, Liu M, Singh KJ, Lin W, et al. Highly stable full-color display device with VLC application potential using semipolar micro-LEDs and all-inorganic encapsulated perovskite nanocrystal. Photonics Research. 2021;**9**(11):2132-2143. DOI: 10.1364/PRJ.431095